Angular Map-Driven Snakes With Application to Object Shape Description in Color Images

Adriana Dumitraş, *Member, IEEE*, and Anastasios N. Venetsanopoulos, *Fellow, IEEE*

***Abstract*—We propose a method for shape description of objects in color images. Our method employs angular maps in order to identify significant changes of color within the image, which are then used to drive snake models. To obtain an angular map, the angle values of the vectors corresponding to color image pixels are first computed with respect to a reference vector, and organized in a two-dimensional matrix. To identify significant color changes within the original image, the edges of the angular map are next extracted. The resulting edge map is then presented to a snake model. Distance and gradient vector flow snake models have been employed in this work. Experimental results show, not only that the resulting object shape descriptions are accurate and quite similar, but also that our method is computationally efficient and flexible.**

***Index Terms*—Angular color map, gradient vector flow, object shape description, snakes.**

I. Introduction

SHAPE description of visual objects is required in many applications such as image and video retrieval, video structuring for browsing and animation [1], cartoon frame filling [2], segmentation [3], and tracking [4]. The shape of an object can be easily described qualitatively by words (using terms such as elongated, rounded, with sharp edges) or by sketches [5]. Describing the shape of an object quantitatively, however, is more difficult and numerous boundary-based and region-based shape description methods have been proposed. Chain codes, geometric border representations, Fourier transforms of the boundaries, polygonal and spline representations, curvature scale-space representations, and deformable (active) models are examples of boundary-based shape methods that have been employed for shape description. Simple scalar region descriptors, moments, region decompositions, and region neighborhood graphs are region-based methods that have been proposed for the same task [1], [5], [6]. Boundary-based active (snake) methods have been particularly successful in describing complex shapes and/or shapes that change dynamically, thereby overcoming the limitations of other shape description methods.

A snake is defined as a curve that evolves within the image until it matches the boundaries of a target object [7], [8]. Snake models have been extensively applied to shape description of objects in bi-level and gray-level images, despite a few problems that are associated with snake initialization and poor convergence to boundary concavities. Snake models have been rarely applied to shape description of objects in color images, with few exceptions[1] such as [9]–[11]. Because they are based on the theory of surface evolution and geometric flows, color snakes of [9]–[11] have quite high computational costs. Therefore, their application to object shape description remains limited. Solutions to apply snake models to color images that likely yield better efficiency consist of:

1) performing color space transforms and then applying snake models to the image planes which contain most of the color information;
2) performing color edge detection and then applying a snake model that is designed for bi-level images to the resulting edge map;
3) including in the snake model terms that depend on the color characteristics of all color planes and applying the snake model to a single image plane;
4) applying snake models separately to each of the color planes [12].

Despite being generally simple, color space transforms are computationally expensive and increase the processing time that is associated to the description of the object shape [13]. Color edge detection applied to the original image is impractical in applications that require processing of mixed databases, which consist of bi-level, gray-level, and color images. Defining color-based terms for the snake models is generally difficult and it is a topic of ongoing research. Applying parametric snake models separately to each color plane has been considered of limited use [9], because of the difficulty in combining the resulting snake shapes into a final contour of the object shape. Although methods that successfully combine the snake shapes obtained in each of the color planes have been proposed [12], they still require processing of all of the image planes. Of course, this is time consuming when processing based on sequential implementations is employed.

To address the above problems, in this work we propose a shape description method of objects in color images using angular map-driven snakes. In our method, the angle value of each vector corresponding to a pixel in the color image is computed, the resulting angle values are next assembled in an angular map, which is then used to drive snake models. Distance snake models [14] and gradient vector flow snake models [15] are selected in

Manuscript received November 10, 2000; revised September 17, 2001. This work was performed at the University of Toronto, Toronto, ON, Canada, and was supported by the Natural Sciences and Engineering Research Council of Canada (NSERC) and the University of Toronto. The associate editor coordinating the review of this manuscript and approving it for publication was Dr. Mark S. Drew.

A. Dumitraş is with AT&T Labs Research, Middletown, NJ 07748 USA (e-mail: adriana@research.att.com).

A. N. Venetsanopoulos is with the Edward Rogers, Sr. Department of Electrical and Computer Engineering, University of Toronto, Toronto, ON M5S 3G4, Canada (e-mail: anv@dsp.toronto.edu).

Publisher Item Identifier S 1057-7149(01)10570-1.

[1]We note that, these works introduce geometrical snake models. All of the other snake models we refer to, as well as those selected in this work, are parametric snake models.

this work, and they are driven by two versions of the angular map.

By making available color information to the snake models and by inheriting the capabilities of the distance and gradient vector flow snake models, respectively, our angular map-based shape description method is clearly effective. Moreover, our proposed method is efficient because 1) it avoids color space transforms, color edge detection, and processing of multiple color planes; 2) it makes use of snake models which can be equally applied to bi-level, gray-level, or color images in a database of mixed pictures; and 3) it makes use of an angular map which is either available (for instance, in applications such as color-based image and video retrieval) or may be computed efficiently using a specified region-of-interest within the image. Finally, our method is flexible, in the sense that the angular map may be computed with respect to different reference vectors. This allows precise and coarse descriptions of object boundaries of higher and lower interest, respectively, by the snake models. Object shape description in medical images, for instance, would particularly benefit from the flexibility of our proposed method, as different parts of the object boundaries (e.g., tumor) may require more accurate descriptions than others for diagnostic purposes.

The rest of the paper is divided in five sections. Section II presents main ideas related to the snake models. Section III provides a detailed presentation of our proposed angular map-driven snake method. Experimental results and conclusions are included in Sections IV and V, respectively.

II. Background

Numerous snake models and variations have been proposed since Kass *et al.* introduced their (today known as traditional) snake model in [7]. Traditional parametric snake models are curves that are described by $\mathbf{z}(s) = (x(s), y(s))$, where x, y, are the coordinates of the snake curve within the image, and s is a parameter which is proportional to the arc length of the snake curve [7]. A snake iteratively changes its position according to the minimization of an energy function given by

$$\begin{aligned} E(\mathbf{z}) &= \int_0^1 E_{int}(\mathbf{z}(s))\,ds + \int_0^1 E_{ext}(\mathbf{z}(s))\,ds \\ &= \frac{1}{2}\int_0^1 \left(\alpha(s)\left|\frac{\partial \mathbf{z}(s)}{\partial s}\right|^2 + \beta(s)\left|\frac{\partial^2 \mathbf{z}(s)}{\partial s^2}\right|^2\right) ds \\ &\quad + \int_0^1 E_{ext}(\mathbf{z}(s))\,ds \end{aligned} \tag{1}$$

where E_{int}, E_{ext}, $\alpha(s)$, and $\beta(s)$ are the internal energy, the external energy, the snake tension, and the snake rigidity, respectively. Typically, the external energy is given by $E_{ext} = I(x, y)$ and $E_{ext} = -|\nabla I(x, y)|^2$ for bi-level and gray-level images, respectively, where $I(x, y)$ and ∇ stand for the original image or the original image convolved with a two-dimensional Gaussian function, and the Laplace operator, respectively.

The snake that minimizes the energy functional $E(\mathbf{z})$ in (1) must satisfy the Euler equation $\mathbf{F}_{int} + \mathbf{F}_{ext} = 0$, where the internal force $\mathbf{F}_{int}$, the external force $\mathbf{F}_{ext}$, α, and β are given by $\mathbf{F}_{int} = \alpha(s)(\partial^2 \mathbf{z}(s)/\partial s^2) - \beta(\partial^4 \mathbf{z}(s)/\partial s^4)$, $\mathbf{F}_{ext} = -\nabla E_{ext}$, $\alpha(s) = \alpha$, and $\beta(s) = \beta$, respectively [7], [15], [16].

Fig. 1. Block diagram of the angular map-driven snake system for object shape description in color images.

Traditional snakes have difficulties to converge to the actual object contours when 1) the initial snake is located far from the object boundaries and 2) the object boundary includes concave sections. To address the first problem, numerous solutions have been proposed, such as the distance snake model [14], the balloon snake model [16], and the dynamic programming-based snake model [17]. To address the second problem, directional [18] and gradient vector flow [15] snake models have been introduced. A comparison of the performances of snake models has been presented in [19], showing that distance snakes and gradient vector flow snakes outperform other snake models in terms of accuracy of the object shape description.

III. Proposed Method

Our goal is to obtain an accurate and flexible shape description of objects in color images with reasonable computational costs. To achieve our goal, we propose an angular map-driven snake method, which is illustrated in Fig. 1. In what follows, we describe each of its processing stages.

Let a color image be represented by a set of two-dimensional image planes in a selected color space. Let each of these image planes be represented as a matrix, each matrix element $M, (x, y)$ consisting of a pixel value in row x and column y [20], [21]. The proposed method consists of three steps. First, we compute the values of an angular color map, which are given by

$$\theta_1(x, y) = 1 - \frac{2}{\pi}\arccos\left(\frac{\mathbf{v}_{(x,y)}\,\mathbf{v}_{ref}}{\|\mathbf{v}_{(x,y)}\|\,\|\mathbf{v}_{ref}\|}\right) \tag{2}$$

or by

$$\theta_2(x, y) = \theta_1(x, y)\left[1 - \frac{\|\mathbf{v}_{(x,y)} - \mathbf{v}_{ref}\|}{\sqrt{3 \times 255^2}}\right] \tag{3}$$

yielding the angular maps $\{\theta_1\}$ or $\{\theta_2\}$, respectively. Notation $\mathbf{v}_{(x,\,y)}$ stands for a vector consisting of the values of all of the pixels located at the position (x, y) within the color image planes. For instance, $\mathbf{v}_{(x,\,y)}$ is the vector $\mathbf{v}_{(x,\,y)} = [R(x, y)\,G(x, y)\,B(x, y)]$ in the RGB color space, where $R(x, y)$, $G(x, y)$, and $B(x, y)$ denote the values of the pixels located at the position (x, y) in the R, G, and B color planes, respectively. Notations $\mathbf{v}_{ref}$, θ_1, and θ_2 stand for a reference vector, the value of the angle given by (2) between the vector $\mathbf{v}_{(x,\,y)}$ and the reference vector $\mathbf{v}_{ref}$, and the value of the angle given by (3) between the vector $\mathbf{v}_{(x,\,y)}$ and the reference vector $\mathbf{v}_{ref}$, respectively.

Second, we identify significant color changes within the original image by extracting the edges of the angular map. Third, the resulting edge map $f(x, y)$ is presented to a snake model in order to obtain a shape description of the color object. In this work, we select distance [14] and gradient vector flow [15] snake models for our object shape description.

If a distance snake model [14] is selected, a potential function which depends on the distance $\mathbf{d}(s)$ between the snake points and the closest edge points of the edge map $f(x, y)$, can be computed. Using the Euclidean distance, this potential function is given by $P(\mathbf{d}(s)) = \sum_i \|z(s_i) - f(x_i, y_i)\|^2$, where $z(s_i)$ is given by $z(s_i) = (x(s_i), y(s_i))$. The external force $\mathbf{F}_{ext}$, which is computed as the negative gradient of the potential function $P(\mathbf{d}(s))$, is obtained by $\mathbf{F}_{ext} = -\nabla P$. Of course, in the case of a Cartesian curve, $x(s_i) = x_i$, $y(s_i) = y_i$, $z(s_i) = (x_i, y_i)$, $d(s_i) = d(x_i, y_i)$, and $\mathbf{F}_{ext}(x, y) = -\nabla P(d(x, y))$. Using the external force $\mathbf{F}_{ext}$, the position of the snake curve is changed iteratively such that an energy functional, such as that of the traditional snake model in Section II, is minimized.

If a gradient vector flow snake model [15] is selected, the external force cannot be written as the negative gradient of a potential function. Instead, the external force of the gradient vector flow snake model is defined by $\mathbf{F}_{ext} = \mathbf{z}(x, y)$, where $\mathbf{z}(x, y) = (u(x, y), v(x, y))$ is a gradient vector flow field, that is, a vector field which minimizes the energy functional given by

$$E(\mathbf{z}) = \iint \mu(u_x^2+u_y^2+v_x^2+v_y^2)+|\nabla f|^2|\mathbf{z}-\nabla f|^2\, dx\, dy. \quad (4)$$

Notations $f(x, y)$ and μ stand for the edge map computed using the angular map and a regularization parameter, respectively. The gradient vector flow field is obtained directly by solving numerically the Euler equations given by [15]

$$\mu\nabla^2 u - (u - f_x)(f_x^2 + f_y^2) = 0 \quad (5)$$

$$\mu\nabla^2 v - (v - f_y)(f_x^2 + f_y^2) = 0. \quad (6)$$

The position of the gradient vector flow snake curve is changed iteratively such that the energy functional given by (4) is minimized.

To summarize, the algorithm described earlier computes an angular map image plane which characterizes the original multiplane color image. This angular map illustrates color changes within the original image, which are then provided to the snake model. We note that, the angular map $\{\theta_1\}$, consisting of values given by (2), has been employed previously in the context of vector filtering, edge detection and color-based image retrieval. We also note that, the angular map $\{\theta_2\}$ is computed using a modified version of the angular distance measure[2] introduced in [22] in the context of color-based image retrieval. In modifying the angular distance of [22] by retaining only the weighted angle term (i.e., we have been motivated by the fact that, the angular map $\{\theta_2\}$ not only has to allow the identification of color discontinuities within the image, but also it has to allow meaningful comparisons of the results with those obtained by the angular map $\{\theta_1\}$. Therefore, the value of θ_2 given by (3) is the same as that of θ_1 given by (2) (that is, zero), for vectors $\mathbf{v}$ that are orthogonal with the reference vector $\mathbf{v}_{ref}$. For vectors $\mathbf{v}$ that are collinear to the reference vector $\mathbf{v}_{ref}$, the values of θ_2 are less than one, because of the weighting factor which is dependent on the magnitudes of the vectors being compared, while the value of θ_1 is equal to 1.

Clearly, the main difference between the angular maps $\{\theta_1\}$ and $\{\theta_2\}$ is the fact that the former takes into account only the angle of the color vectors, whereas the latter takes into account both the angle and the magnitude of the color vectors. Both angular maps $\{\theta_1\}$ and $\{\theta_2\}$, however, indicate color changes within the image. We can illustrate this by using two simple examples. In the first example, which is illustrated in Fig. 2(a), a blue circle is placed on a green background. Both graphical representations of the angular maps $\{\theta_1\}$ and $\{\theta_2\}$ show that, the color changes in the image correspond to the object boundary. To further illustrate the effectiveness of the color angular maps, a second example is provided in Fig. 2(b). By contrast to Fig. 2(a), we here employ the image BREAM, which contains several colors. Even so, the object boundary is correctly identified using both of the color angular maps and it is shown more clearly in the graphical representation of the angular map $\{\theta_1\}$.

In the examples illustrated in Fig. 2, both angular maps have been computed with respect to the reference vector $\mathbf{v}_{ref} = [1\,1\,1]$. When *a priori* knowledge regarding the color content of the image is available, other reference vectors may be selected, which may enhance significantly the angular map values corresponding to the object boundaries. More specifically, by selecting a different reference vector, the angular maps will yield more accurate information for some of the object outline segments, while yielding less accurate information about others. This is illustrated in Fig. 3. The boundaries of the blue circle on a half-green and half-red background are more visible when the reference vectors are selected to be equal to $\mathbf{v}_{ref} = [1\,0\,0]$ (red) or $\mathbf{v}_{ref} = [0\,1\,0]$ (green). We also note that, this is even more clear in the graphical representation of the angular map $\{\theta_1\}$, whereas in that of $\{\theta_2\}$, the weighting term which depends on the magnitudes of the vectors being compared, contributes to reducing this effect.

Simple gray-level edge detection may be applied to the resulting angular maps in order to detect color changes within the original image. This solution has several advantages. By applying edge detection to a single image plane, computational costs of methods such as [23], [24], which identify directions of major changes in vector data, are avoided. Moreover, an initial approximation of the object boundary is not required for the computation of the edge map, as compared to methods such as [25], which compute color variations by differences between inside and outside contour points. Finally, in image databases that contain both gray-level and color images, it is particularly convenient to apply the same edge detection tool to the original image and angular map, respectively.

[2]The normalization constant equal to $\sqrt{3 \times 255^2}$ in (3) is the same as that selected in [22], and it is selected to be equal to the magnitude of the maximum difference vector (i.e., [255 255 255]) which may be obtained in the RGB color space.

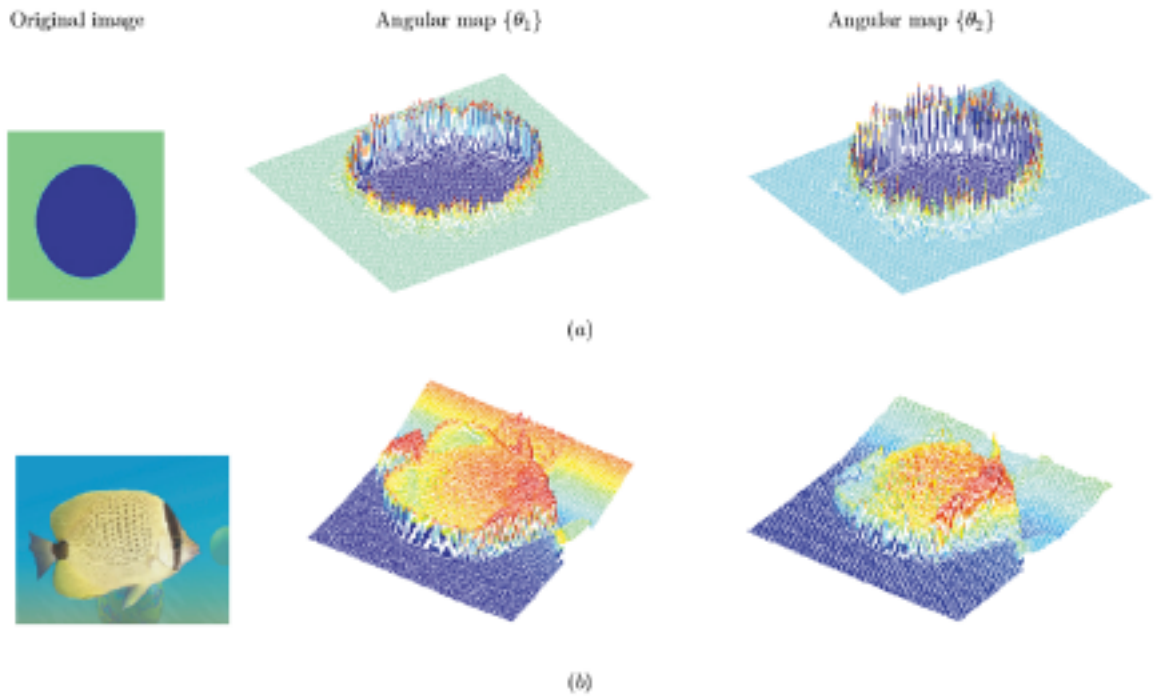

Fig. 2. Simple example using: (a) a blue circle on a green background and (b) the image BREAM. The angular maps $\{\theta_1\}$ and $\{\theta_2\}$ have been computed using (2) and (3), respectively. Different angle values are represented using different colors in each of the angular maps.

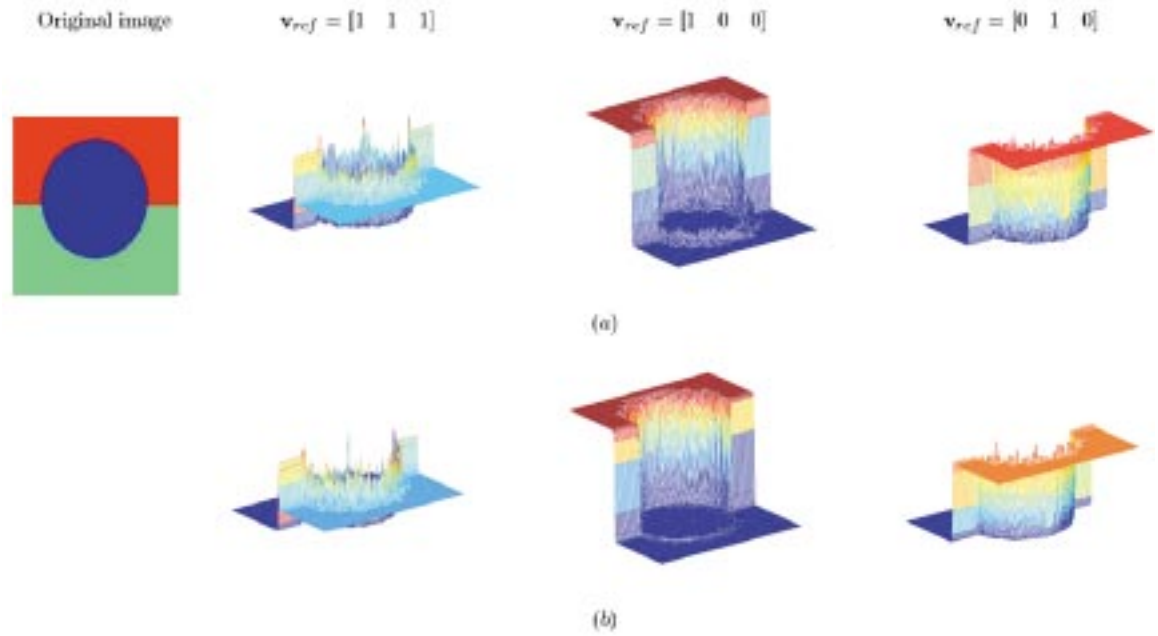

Fig. 3. Simple example using a blue circle on a half-green and half-red background and different reference vectors $\mathbf{v}_{ref}$. The angular maps (a) $\{\theta_1\}$ and (b) $\{\theta_2\}$ have been computed using (2) and (3), respectively. Different angle values are represented using different colors in each of the angular maps.

IV. EXPERIMENTAL RESULTS

In what follows, we illustrate the performance, flexibility, and computational advantages of our proposed angular map-driven snake method for object shape description.

A. Implementation Details

Several implementation issues need to be addressed before illustrating the performance of our method, namely the image test set, the color space, the initialization conditions, the parameter values, the number of iterations, the computation of the edge maps and the evaluation indexes. The images used in our experiments are color frames from the video sequence BREAM and the color pictures SEAGULL, HIBISCUS and ROSE from the Kodak image set [26]. The shapes of the objects within these images contain smooth and high detail, as well as convex and concave segments.

Our images are represented in the RGB, normalized RGB and opponent color spaces. The representation in the RGB color

Fig. 4. Performance of the distance snake in the (a) RGB, (b) normalized RGB, and (c) opponent color spaces using the angular color map $\{\theta_1\}$ given by (2) and the color images BREAM, SEAGULL, HIBISCUS, and ROSE. The final snakes are superimposed over the original images.

Fig. 5. Performance of the gradient vector flow snake in the (a) RGB, (b) normalized RGB, and (c) opponent color spaces using the angular color map $\{\theta_1\}$ given by (2) and the color images BREAM, SEAGULL, HIBISCUS, and ROSE. The snakes are superimposed over the original images.

space is motivated by the fact that, images are most frequently stored as such. The representation in the normalized RGB color space, which consists of normalized colors (chromaticity coordinates) that are given by the nonlinear transform $r = R/(R+G+B)$, $g = G/(R+G+B)$, and $b = B/(R+G+B)$ of the R, G, and B color planes, respectively, is also commonly used because the normalized colors have better stability with respect to illumination changes than their R, G, and B correspon-

dents. The representation in the opponent color space, which assumes that the channels red–green (RG), yellow–blue (YB), and white–black (achromatic, WB) exist and are given by the nonlinear transform $RG = R - G$, $YB = 2B - R - G$, and $WB = R + G + B$ of the R, G, and B color planes, respectively, is quite frequently employed as well [20].

We initialize the snake models using user-defined polygonal regions-of-interest,[3] although any shape of region-of-interest may be selected. The parameter values and the number of iterations are the same in all of our experiments and they are equal to $\alpha = 0.05$, $\beta = 0$, and $\mu = 0.2$, where α, β and μ are the elasticity, rigidity and regularization parameters of the gradient vector flow snake model, respectively [15]. The number of iterations has been selected to be equal to 500. The edge maps are computed using Sobel edge detectors for all of the angular maps.

We evaluate the accuracy of the shape contours subjectively and objectively. More specifically, we perform visual inspection of the shape contours and we compute the normalized perimeter and the normalized surface-area of the snake object [27], and the normalized number of missed pixels. The normalized perimeter is computed as the ratio between the snake object perimeter and the actual object perimeter. The normalized surface-area is computed as the ratio between the snake object surface-area[4] and the actual object surface-area. The normalized number of missed pixels is computed as the ratio between the number of missed pixels and the actual object surface-area.

B. Results

We compute the values of the angular map $\{\theta_1\}$ given by (2). Next, we present the edge image plane obtained using the resulting angular map to the snake model. Figs. 4 and 5 illustrate the shape descriptions obtained using distance and gradient vector flow snake models, respectively, and the test images in the RGB, normalized RGB and opponent color spaces. The angular map has been computed with respect to the reference vector $\mathbf{v}_{ref} = [1\,1\,1]$ for Fig. 4(a) and (b), and Fig. 5(a) and (b), and $\mathbf{v}_{ref} = [1\,0\,0]$ for Fig. 4(c) and Fig. 5(c), respectively. As these figures illustrate, the accuracy of the gradient vector flow snake model is higher than that of the distance snake model. This is also confirmed by the values of the objective indexes[5] in Tables I and II. The normalized number of missed pixels decreases for the snake object boundaries obtained by the gradient vector flow snake as compared to those obtained by the distance snake for all of the images. Moreover, each of the snake models yields almost identical shape descriptions for the same image object in both RGB and normalized RGB color spaces. In general, the shape description results improve when the images are represented in the opponent color space, as shown in Figs. 4 and 5, and Tables I and II. This is mostly visible in Fig. 4(c) and Fig. 5(c) for the image ROSE, which is particularly difficult to process by the snake models because of the object of interest (the rose) being located behind a fence (which yields strong edges within the image). In the opponent color space, both snake models identify correctly most of the rose boundary, as opposed to the RGB and normalized RGB color spaces, where the snake models are sometimes attracted to the fence edges.

TABLE I
THE NORMALIZED PERIMETER $\mathcal{P}$, THE NORMALIZED SURFACE-AREA $\mathcal{A}$ OF THE SNAKE OBJECT, AND THE NUMBER $\mathcal{N}$ OF MISSED PIXELS FOR THE IMAGES ILLUSTRATED IN FIG. 4. THE ANGULAR MAP $\{\theta_1\}$ GIVEN BY (2) AND THE DISTANCE SNAKE HAVE BEEN EMPLOYED

Color space	Evaluation index	Image			
		BREAM	SEAGULL	HIBISCUS	ROSE
RGB	$\mathcal{P}$	0.860	0.777	0.887	1.029
	$\mathcal{A}$	1.033	0.998	1.098	0.953
	$\mathcal{N}$	0.088	0.136	0.148	0.185
Normalized RGB	$\mathcal{P}$	0.860	0.790	0.885	1.029
	$\mathcal{A}$	1.033	0.999	1.098	0.953
	$\mathcal{N}$	0.088	0.137	0.147	0.185
Opponent	$\mathcal{P}$	0.843	0.811	0.971	1.010
	$\mathcal{A}$	1.044	0.969	1.038	1.019
	$\mathcal{N}$	0.065	0.072	0.104	0.128

TABLE II
THE NORMALIZED PERIMETER $\mathcal{P}$, THE NORMALIZED SURFACE-AREA $\mathcal{A}$ OF THE SNAKE OBJECT, AND THE NUMBER $\mathcal{N}$ OF MISSED PIXELS FOR THE IMAGES ILLUSTRATED IN FIG. 5. THE ANGULAR MAP $\{\theta_1\}$ GIVEN BY (2) AND THE GRADIENT VECTOR FLOW SNAKE HAVE BEEN EMPLOYED

Color space	Evaluation index	Image			
		BREAM	SEAGULL	HIBISCUS	ROSE
RGB	$\mathcal{P}$	0.931	0.845	0.963	0.955
	$\mathcal{A}$	1.013	0.989	1.061	1.027
	$\mathcal{N}$	0.034	0.065	0.092	0.182
Normalized RGB	$\mathcal{P}$	0.931	0.845	0.963	0.932
	$\mathcal{A}$	1.013	0.989	1.061	1.043
	$\mathcal{N}$	0.034	0.065	0.092	0.166
Opponent	$\mathcal{P}$	0.956	0.822	1.081	0.979
	$\mathcal{A}$	1.015	0.967	0.977	0.979
	$\mathcal{N}$	0.048	0.071	0.093	0.117

Similar results to those illustrated in Figs. 4 and 5 have been obtained using the angular map $\{\theta_2\}$ given by (3), when the reference vectors have been selected to be identical to those mentioned above. This is, of course, motivated by the fact that, in this case the angular maps given by (2) and (3) yield identical values. When different values of the reference vectors are selected, however, the performance of the gradient vector flow snake model using the image ROSE is better than that of the distance snake model. Moreover, as Fig. 6 shows, the performance of the gradient vector flow snake model using the angular map $\{\theta_1\}$ is better than that obtained using the angular map $\{\theta_2\}$. The shape descriptions obtained using images represented in the RGB and normalized RGB color spaces are quite similar, and they are consistently outperformed by those obtained using the same images represented in the opponent color space.

To illustrate the impact of the reference vector on the accuracy of the resulting shape description, we have selected numerous values of $\mathbf{v}_{ref}$ in our experiments. Fig. 6 illustrates a simple example. By selecting the reference vector to be $[0\,1\,0]$, the shape description obtained by the gradient vector flow snake model using the image ROSE in the opponent color space and the angular map $\{\theta_1\}$ is more accurate than that in Fig. 5(c). In the

[3]The assumption that a region-of-interest is available is valid in light of the numerous applications which require either a coarse approximation of the object location or a user-defined region-of-interest.

[4]The surface-area of the object is defined as the total number of pixels within the actual object.

[5]For perfect shape descriptions, the normalized perimeter is equal to one, the normalized surface-area is also equal to one, and the normalized number of missed pixels is equal to zero.

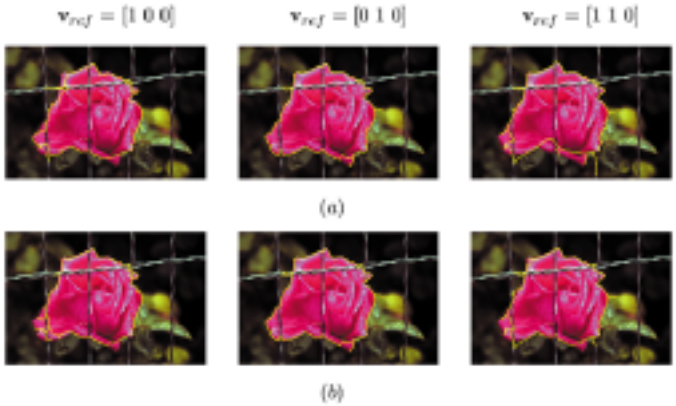

Fig. 6. Performance of the gradient vector flow snake in the opponent color space using (a) the angular map $\{\theta_1\}$ given by (2) and (b) the angular map $\{\theta_2\}$ given by (3), and the color image ROSE. The snakes are superimposed over the original image.

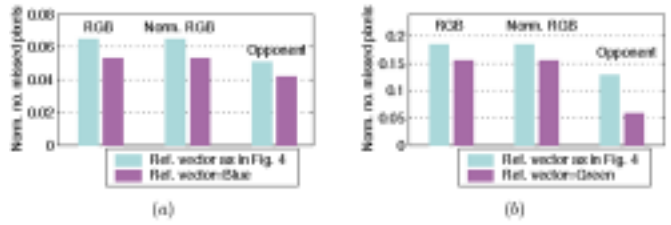

Fig. 7. Normalized number of missed pixels for the snake boundary descriptions of the objects (a) SEAGULL and (b) ROSE, when the reference vector is selected as in Fig. 4, or as the dominant color. The angular map $\{\theta_1\}$ and the gradient vector flow snake model have been employed.

RGB and normalized RGB color spaces, the numbers of missed pixels are also consistently reduced by selecting the reference vector as the dominant color, as Fig. 7 illustrates for the images ROSE and SEAGULL. Similar results hold for shape descriptions obtained using the angular map $\{\theta_2\}$. For this angular map and selections of the reference vector which are close to the mean vector of the image, the resulting shape descriptions and the normalized numbers of missed pixels are included in Table III. Clearly, the reference vectors $\mathbf{v}_1$ and $\mathbf{v}_2$, which are the closest to the mean vectors of the images BREAM and ROSE, respectively, yield angular maps which in turn, lead to the most accurate shape descriptions of those included in the table. Finally, we note that, even when the reference vector is selected incorrectly,[6] as in the right-most column of Fig. 6, the resulting shape description still matches partially the object boundaries.

The CPU times required by the computation of the angular maps $\{\theta_1\}$ and $\{\theta_2\}$, distance potential forces and gradient vector flow forces, respectively, for a typical image of size equal to 256×256 pixels, are included in Table IV. For such an image size, the computation of the angular map $\{\theta_1\}$ is approximately two times faster than that of the angular map $\{\theta_2\}$. We note that, in numerous applications, such as color-based image retrieval using angular distance measures, the angular map may be already available. When the angular map is not available, however, it is efficient as well as sufficient (especially for medium to large images) to compute it within a specified region-of-interest. As Table IV also shows, the CPU time required by the computation of the angular map values for a typical region-of-interest employed in our experiments decreases significantly as compared to that required by its computation using the entire image, again in favor of the angular map $\{\theta_1\}$. Moreover, the CPU time required by the computation of the distance potential forces and gradient vector flow forces for a region-of-interest is approximately the same, therefore the selection of either of the two snake models has the same impact on the proposed method.

[6]For images represented in the opponent color space, the RG and BY components are mutually exclusive [20].

TABLE III
THE NORMALIZED NUMBER $\mathcal{N}$ OF MISSED PIXELS FOR THE SNAKE OBJECTS OBTAINED USING THE ANGULAR MAP $\{\theta_2\}$ GIVEN BY (3), DIFFERENT REFERENCE VECTORS, THE GRADIENT VECTOR FLOW SNAKE MODEL, AND THE IMAGES BREAM AND ROSE. IN (3), THE VALUES OF θ_2 HAVE BEEN COMPUTED USING THE VECTORS $\mathbf{v}_{ref}$ AND $\mathbf{v}_{mean}$, WHERE $\mathbf{v}_{mean}$ IS THE MEAN VECTOR OF EACH OF THE IMAGES. THE VECTORS INCLUDED IN THE TABLE HAVE ALREADY BEEN NORMALIZED

Image	Reference vector		
	$\mathbf{v}_1 = [0\ 0.3\ 0.7]$	$\mathbf{v}_2 = [0\ 0.7\ 0.3]$	$\mathbf{v}_3 = [0\ 0.9\ 0.9]$
BREAM	$\theta_2 = 0.432$	$\theta_2 = 0.453$	$\theta_2 = 0.506$
	$\mathcal{N} = 0.050$	$\mathcal{N} = 0.065$	$\mathcal{N} = 0.080$
			
ROSE	$\mathbf{v}_1 = [0.3\ 0.7\ 0]$	$\mathbf{v}_2 = [0.7\ 0.3\ 0]$	$\mathbf{v}_3 = [0.9\ 0.9\ 0]$
	$\theta_2 = 0.265$	$\theta_2 = 0.538$	$\theta_2 = 0.275$
	$\mathcal{N} = 0.237$	$\mathcal{N} = 0.144$	$\mathcal{N} = 0.279$
			

TABLE IV
CPU TIME [SEC] REQUIRED BY THE COMPUTATION OF $\{\theta_1\}$, $\{\theta_2\}$, DISTANCE POTENTIAL FORCES AND GRADIENT VECTOR FLOW FORCES, USING A 664 MHz PENTIUM III PC. NOTATIONS $\{\theta_1\}$ AND $\{\theta_2\}$ STAND FOR THE ANGULAR MAPS GIVEN BY (2) AND (3), RESPECTIVELY; ROI DENOTES A USER SPECIFIED REGION-OF-INTEREST

CPU time for computing	256×256 image	185×185 ROI
Angular map $\{\theta_1\}$	171.14	11.77
Angular map $\{\theta_2\}$	348.16	52.38
Distance potential forces	131.11	24.72
GVF forces	45.97	26.50

C. Discussion

In this section, we comment on the accuracy, flexibility, and computational demands of our proposed method. The accuracy of the resulting object shape description depends on the selection of the angular map, color space, reference vector, and snake model. In terms of accuracy, both angular maps $\{\theta_1\}$ and $\{\theta_2\}$ yield good descriptions of the object shape. The results obtained using the angular map $\{\theta_1\}$, however, outperform those obtained using the angular map $\{\theta_2\}$. This is motivated by the fact that, the values of $\{\theta_2\}$ are weighted angle values. By contrast, the values of $\{\theta_1\}$ are angle values without weighting. Consequently, $\{\theta_1\}$ indicates more visibly the color changes. As such, for shape description purposes, the angular map $\{\theta_1\}$

should be selected, whereas for other applications which make use of the angle *and* the magnitude of the color vectors, such as color-shape-based image retrieval, $\{\theta_2\}$ should be employed.

The selection of images represented in the RGB and normalized RGB color spaces yields similar shape descriptions when using the same angular map. This is motivated by the fact that, the orientation of the vectors corresponding to the color images represented in these color spaces is essentially the same. When the images are represented in the opponent color space, the resulting shape descriptions outperform those obtained using the same images represented in the RGB and normalized RGB color spaces. This is motivated by the fact that, the opponent color space contains less redundancy[7] in the color channels than that of each of the other two color spaces, and color changes in terms of angle are more visible in separate color image planes.

The selection of the reference vector as a dominant color in the image led to accurate descriptions of the object shapes in our experiments. Moreover, as illustrated in Fig. 3, where either the upper or the lower sections of the circle object boundaries is described better, partially accurate and partially coarse shape descriptions of the object have also been obtained. All of these selections of the reference vector require *a priori* knowledge regarding the color content of the image. Medical imaging applications may especially make use of this information for shape description purposes, because the color of the tissue which is adjacent to the object contour (tumor) is typically known, thereby the reference vector may be selected as mentioned above. When *a priori* information about the image content is not available, the reference vector may be selected simply as the mean vector of the image, as a vector close to the mean vector, or even as the vector $[1\ 1\ 1]$ (in the RGB or normalized RGB color spaces), or as the vector $[1\ 0\ 0]$ (in the opponent color space). As shown in Section IV-B, these selections yield angular maps which allow correct identification of the color changes within the image. We have shown that, even if the reference vector is selected incorrectly, the resulting shape description may still be acceptable, as it matches partially the object boundaries. The fact that, the reference vector may be selected such that different accuracies of the resulting shape descriptions are obtained, shows the flexibility of our proposed method.

The distance snake model yields similar performance to that of the gradient vector flow snake model. As expected, the latter snake model has better ability to fill in the concave sections of the object boundary than the former model. The gradient vector flow snake model is also more robust with respect to incorrect selections of the reference vectors. While they yield similar object shape descriptions, the distance and gradient vector flow snake models have quite different computational demands for typical image sizes. More specifically, the computation of the gradient vector flow snake forces is faster than that of the distance potential forces. We note, however, that these snake models yield similar efficiency in terms of speed when applied to smaller regions-of-interest within the image. Consequently, it is the selection of the angular map that has a strong impact on the overall speed of our angular map-driven snake method. The selection of the angular map $\{\theta_1\}$ yields higher speed of our proposed method, than that of the angular map $\{\theta_2\}$. Moreover, when viewed in a general sense, as the application of a transform to a color image, the computation of the angular map given by (2) or (3) also requires less computational resources than color space transforms such as RGB to HSV, or RGB to CIELAB [13].

[7]More specifically, as a consequence of the arrangement of colors in the opponent color space, all colors may be described as containing red or as containing green, but never as containing both colors simultaneously [20].

V. Conclusions

We have proposed an angular-map driven snake method for object shape description in color images. By making use of color information and the abilities of selected (distance or gradient vector flow) snake models, our method is highly effective. By avoiding color space transforms, color edge detection, and processing of multiple color planes, and by using snake models that can be also applied to bi-level or gray-level images, our method is also efficient. By making use of an angular map which is either available or may be computed easily using various reference vectors, our method is flexible. As such, the proposed angular-map drive snake method is well suited to numerous applications that require object shape description in color images, including image database retrieval and medical imaging.

References

[1] M. Safar, C. Shahabi, and X. Sun, "Image retrieval by shape: A comparative study," Dept. Comput. Sci., Univ. Southern California, Los Angeles, Tech. Rep. 99-719; available on the Internet, Nov. 1999.

[2] A. K. Jain, Y. Zhong, and S. Lakshmanan, "Object matching using deformable templates," *IEEE Trans. Pattern Anal, Machine Intell.*, vol. 18, pp. 267–278, Mar. 1996.

[3] S. C. Zh and A. Yuille, "Region competition: Unifying snakes, region growing, and Bayes/MDL for multiband image segmentation," *IEEE Trans. Pattern Anal. Machine Intell.*, vol. 18, pp. 884–900, Sept. 1996.

[4] F. Leymarie and M. D. Levine, "Tracking deformable objects in the plane using and active contour model," *IEEE Trans. Pattern Anal. Machine Intell.*, vol. 15, pp. 617–634, June 1993.

[5] M. Sonka, V. Hlavac, and R. Boyle, *Image Processing, Analysis and Machine Vision*. London, U.K.: Chapman & Hall, 1993.

[6] F. Mokhtarian and A. K. Mackworth, "A theory of multiscale, curvature-based shape representation for planar curves," *IEEE Trans. Pattern Anal. Machine Intell.*, vol. 14, pp. 789–805, Aug. 1992.

[7] M. Kass, A. Witkin, and D. Terzopoulos, "Snakes: Active contour models," *Int. J. Comput. Vis.*, vol. 1, pp. 321–331, 1988.

[8] D. Androutsos, P. E. Trahanias, and A. N. Venetsanopoulos, "Application of active contours for photochromic tracer flow extraction," *IEEE Trans. Med. Imag.*, vol. 16, pp. 284–293, June 1997.

[9] G. Sapiro, "Color snakes," Hewlett-Packard Labs, Palo Alto, CA, Tech. Rep. HP-95-113, Aug. 1995.

[10] ——, "Vector (self) snakes: A geometric framework for color, texture, and multiscale image segmentation," in *Proc. IEEE ICIP*, vol. 1, 1996, pp. 817–820.

[11] G. Sapiro and D. L. Ringach, "Anisotropic diffusion of multivalued images with application to color filtering," *IEEE Trans. Image Processing*, vol. 5, pp. 1582–1586, Nov. 1996.

[12] A. Dumitraş and A. N. Venetsanopoulos, "Multicolored snakes in the RGB color space," in *Proc. IEEE PCM*, Sydney, Australia, 2000, pp. 240–244.

[13] C. Connolly and T. Fliess, "A study of efficiency and accuracy in the transformation from RGB to CIELAB color space," *IEEE Trans. Image Processing*, vol. 6, pp. 1046–1048, July 1997.

[14] L. D. Cohen and I. Cohen, "Finite-element methods for active contour models and balloons for 2-D and 3-D images," *IEEE Trans. Pattern Anal. Machine Intell.*, vol. 15, pp. 1131–1147, Nov. 1993.

[15] C. Xu and J. L. Prince, "Snakes, shapes, and gradient vector flow," *IEEE Trans. Image Processing*, vol. 7, pp. 359–369, Mar. 1998.

[16] L. D. Cohen, "On active contour models and balloons," *CVGIP, Image Understand.*, vol. 53, pp. 211–218, Mar. 1991.

[17] A. A. Amini, T. E. Weymouth, and R. C. Jain, "Using dynamic programming for solving variational problems in vision," *IEEE Trans. Pattern Anal. Machine Intell.*, vol. 12, pp. 855–867, Sept. 1990.
[18] A. J. Abrantes and J. S. Marques, "A class of constrained clustering algorithms for object boundary extraction," *IEEE Trans. Image Processing*, vol. 5, pp. 1507–1521, Nov. 1996.
[19] A. Dumitraş and A. N. Venetsanopoulos, "A comparative study of snake models with application to object shape description in bi-level and gray-level images," in *Proc. IEEE-EURASIP Workshop NSIP*, Baltimore, MD, 2001.
[20] S. J. Sangwine and E. E. N. Horne, Eds., *The Color Image Processing Handbook*. London, U.K.: Chapman & Hall, 1998.
[21] K. Plataniotis and A. N. Venetsanopoulos, *Color Image Processing and Applications*. New York: Springer-Verlag, 2000.
[22] D. Androutsos, K. Plataniotis, and A. N. Venetsanopoulos, "A novel vector-based approach to color image retrieval using a vector angular-based distance measure," *Comput. Vis. Image Understanding*, vol. 75, pp. 46–58, July/Aug. 1999.
[23] M. Black, G. Sapiro, D. Marimont, and D. Heeger, "Robust anisotropic diffusion and sharpening of scalar and vector images," in *Proc. IEEE ICIP*, vol. 1, 1997, pp. 263–266.
[24] T. Gevers and A. W. M. Smeulders, "PicToSeek: Combining color and shape invariant features for image retrieval," *IEEE Trans. Image Processing*, vol. 9, pp. 102–119, Jan. 2000.
[25] Y. Fu, A. T. Erdem, and A. M. Tekalp, "Occlusion adaptive motion snake," in *Proc. IEEE ICIP*, vol. 3, 1998, pp. 633–637.
[26] Kodak. (2000) Sample digital pictures. [Online]available at www.kodak.com/digitalImages/samples/~samples.shtml
[27] P. Brigger, J. Hoeg, and M. Unser, "B-spline snakes: A flexible tool for parametric contour detection," *IEEE Trans. Image Processing*, vol. 9, pp. 1484–1496, Sept. 2000.
[28] P. E. Trahanias, D. Karakos, and A. N. Venetsanopoulos, "Directional processing of color images: Theory and experimental results," *IEEE Trans. Image Processing*, vol. 5, pp. 868–880, June 1996.

Adriana Dumitraş (SM'98–M'99) received the M.Sc. degree from the "Politehnica" University of Bucharest, Romania, in 1988, and the Ph.D. degrees from the "Politehnica" University and University of British Columbia, Vancouver, BC, Canada, in 1996 and 1999, respectively.

She was a National Sciences and Engineering Research Council of Canada Postdoctoral Fellow with the Department of Electrical and Computer Engineering at the University of Toronto, Toronto, ON, Canada, in 2000. Prior to joining AT&T Labs Research, Middletown, NJ, as a Senior Technical Staff Member, she was a Senior Assistant Professor with the Department of Electronics and Telecommunications at the "Politehnica" University of Bucharest, and held R&D positions with the Vision and Scanning Group of the National Research Council of Canada and Peripheral Equipment Company in Bucharest. Her current research interests are in the areas of content-based and object-based image and video processing. She has coauthored more than 50 journal papers, conference papers, books, book chapters, standards contributions, and technical reports.

Dr. Dumitraş serves as a reviewer of IEEE TRANSACTIONS ON IMAGE PROCESSING, IEEE TRANSACTIONS ON MULTIMEDIA, and IEEE TRANSACTIONS ON CIRCUITS AND SYSTEMS II. She serves as a reviewer for numerous IEEE conferences and as a Session Chair at the IEEE International Conference on Image Processing 2001. She was the Head of the Canadian delegation at ISO/IEC/JTC 1/SC29/WG 11 (MPEG) from December 1998 to July 1999, and a voting member of the Canadian delegation at the same organization from 1998 to 2000, contributing actively to the development of the MPEG-7 Standard. She was the youngest corecipient of the Romanian Academy Award (1996).

Anastasios (Tas) N. Venetsanopoulos (S'66–M'69–SM'79–F'88) received the Diploma of Engineering degree from the National Technical University of Athens (NTU), Greece, in 1965, and the M.S., M.Phil., and Ph.D. degrees in electrical engineering from Yale University, New Haven, CT, in 1966, 1968, and 1969, respectively.

He joined the Department of Electrical and Computer Engineering at the University of Toronto, Toronto, ON, Canada, in September 1968 as a Lecturer and he was promoted to Assistant Professor in 1970, Associate Professor in 1973, and Professor in 1981. Since July 1997, he has been Associate Chair—Graduate Studies of the Department of Electrical and Computer Engineering and was Acting Chair of the Electrical and Computer Engineering Department, during the period of January 1999–July 1999. In 1999, The Bell Canada Chair in Multimedia was established in the ECE Department, made possible by a donation of $1.25 M from Bell Canada, matched by an equal amount of university funds. He assumed this position as Inaugural Chairholder in July 1999. He has served as Chair of the Communications Group and as Associate Chair of the Department of Electrical and Computer Engineering. He was on research leave at the Imperial College of Science and Technology, the National Technical University of Athens, the Swiss Federal Institute of Technology, the University of Florence and the Federal University of Rio de Janeiro, and was Adjunct Professor at Concordia University. He has served as a Lecturer in 138 short courses to industry and continuing education programs and as Consultant to numerous organizations. He is a contributor to 29 books, and is a coauthor of *Nonlinear Digital Filters: Principles and Applications* (Norwell, MA: Kluwer, 1990), *Artificial Neural Networks: Learning Algorithms, Performance Evaluation and Applications* (Norwell, MA: Kluwer, 1993), *Fuzzy Reasoning in Information, Decision and Control Systems* (Norwell, MA: Kluwer, 1994), and *Color Image Processing and Applications* (Berlin, Germany: Springer-Verlag, 1990), and has published more than 650 papers on digital signal and image processing and digital communications. He was Editor of the *Canadian Electrical Engineering Journal* (1981–1983).

Dr. Venetsanopoulos has served as Chair on numerous boards, councils and technical conference committees, including IEEE committees, such as the Toronto Section (1977–1979) and the IEEE Central Canada Council (1980–1982); he was President of the Canadian Society for Electrical Engineering and Vice President of the Engineering Institute of Canada (1983–1986). He was a Guest Editor and Associate Editor for numerous IEEE journals. He is a member of the IEEE Communications, Circuits and Systems, Computer, and Signal Processing Societies, as well as a member of Sigma Xi, the Technical Chamber of Greece, the European Association of Signal Processing, the Association of Professional Engineers of Ontario (APEO) and Greece. He was elected as a Fellow of the IEEE "for contributions to digital signal and image processing," Fellow of EIC, "for contributions to electrical engineering" and was awarded an Honorary Doctorate from the National Technical University of Athens, in October 1994. In October 1996, he was awarded the "Excellence in Innovation Award" of the Information Technology Research Centre of Ontario and Royal Bank of Canada, "for innovative work in color image processing and its industrial applications." In 2000, he was awarded the Millennium Medal of IEEE. Since July 2001, he has been serving as the Dean of the College (Faculty) of Applied Science and Engineering of the University of Toronto.